Eur. Phys. J. B (2015) 88: 160
DOI: 10.1140/epjb/e2015-60168-4

THE EUROPEAN PHYSICAL JOURNAL B

Regular Article

Role of initial correlation in coarsening of a ferromagnet

Saikat Chakraborty and Subir K. Das[a]

Theoretical Sciences Unit, Jawaharlal Nehru Centre for Advanced Scientific Research, Jakkur P.O., 560064 Bangalore, India

Received 4 March 2015 / Received in final form 11 May 2015
Published online 17 June 2015 –

Abstract. We study the dynamics of ordering in ferromagnets via Monte Carlo simulations of the Ising model, employing the Glauber spin-flip mechanism, in space dimensions $d = 2$ and 3, on square and simple cubic lattices. Results for the persistence probability and the domain growth are discussed for quenches to various temperatures (T_f) below the critical one (T_c), from different initial temperatures $T_i \geq T_c$. In long time limit, for $T_i > T_c$, the persistence probability exhibits power-law decay with exponents $\theta \simeq 0.22$ and $\simeq 0.18$ in $d = 2$ and 3, respectively. For finite T_i, the early time behavior is a different power-law whose life-time diverges and exponent decreases as $T_i \to T_c$. The two steps are connected via power-law as a function of domain length and the crossover to the second step occurs when this characteristic length exceeds the equilibrium correlation length at $T = T_i$. $T_i = T_c$ is expected to provide a *new universality class* for which we obtain $\theta \equiv \theta_c \simeq 0.035$ in $d = 2$ and $\simeq$0.105 in $d = 3$. The time dependence of the average domain size ℓ, however, is observed to be rather insensitive to the choice of T_i.

1 Introduction

When a homogeneous system is quenched below the critical point, the system becomes unstable to fluctuations and approaches towards the new equilibrium via the formation and growth of particle rich and particle poor domains [1–4]. In such nonequilibrium evolutions, over several decades, aspects that received significant attention are the domain pattern [3,5–9], rate of domain growth [5,10–15], persistence [16–25] and aging [26–31]. Average size, ℓ, of domains typically grows with time (t) as [5]

$$\ell \sim t^{\alpha}. \tag{1}$$

The value of the exponent α for nonconserved order-parameter dynamics [5,12], e.g., during ordering in a uniaxial ferromagnet, is 1/2, in space dimension $d = 2$. In addition to the interesting structures exhibited by the domains of like spins (or atomic magnets) in a ferromagnet, the unaffected or persistent spins also form beautiful fractal patterns [16–19,21,22]. Typically, fraction of such spins, henceforth will be referred to as the persistent probability, P, decays as

$$P \sim t^{-\theta}, \tag{2}$$

with [20,21] θ having a value $\simeq$0.22 for the Ising model in space dimension $d = 2$ and $\simeq$0.18 in $d = 3$.

The values of the exponents mentioned above are understood to be true for the perfectly random initial configurations, mimicking the paramagnetic phase at temperature $T = \infty$. Another relevant situation is to quench a system from finite initial temperature (T_i) with a large equilibrium correlation length ξ. However, this problem has received only occasional attention [32–35], though experimentally very relevant. In this context, the behavior of the two-time equal point correlation function, relevant in the aging phenomena, was studied [33,34] for $T_i = T_c$, the critical temperature. It was pointed out that such quenches would form a *new universality class* and was shown that the decay of the above correlation was significantly slower for $T_i = T_c$ than $T_i = \infty$. In view of that, a slower decay of P is also expected [35]. On the other hand, the behavior of P and ℓ are expected to be disconnected [36]. Nevertheless, the rate of growth of ℓ may be different for $T_i = T_c$ and $T_i = \infty$, at least during the transient period. In this paper, we address the T_i dependence for persistence and domain growth in a ferromagnet, via Monte Carlo (MC) simulations [37] of nearest neighbor Ising model [37]

$$H = -J \sum_{\langle ij \rangle} S_i S_j; \; S_i = \pm 1, \; J > 0, \tag{3}$$

in $d = 2$ and $d = 3$, on square and simple cubic lattices, respectively.

Starting from a high value, as T_i approaches T_c [37] ($\simeq 2.27 J/k_B$ in $d = 2$ or $4.51 J/k_B$ in $d = 3$, k_B being the Boltzmann constant), a two-step decay in P becomes prominent, except for $T_i = T_c$. For the latter initial temperature, power-law behavior with exponents much smaller than the ones observed for quenches from $T_i = \infty$ lives forever. In addition to identifying these facts, a primary objective of the paper is to accurately quantify these decays and find out the influence of dimensionality. For the

[a] e-mail: das@jncasr.ac.in

domain growth, on the other hand, we do not observe a modification to the time dependence with the variation of T_i, *almost* from the very beginning.

The rest of the paper is organized as follows. In Section 2 we briefly describe the methods. Results from both the dimensions are presented in Section 3. Section 4 concludes the paper with a summary and outlook.

2 Methods

The nonconserved order-parameter dynamics in the MC simulations have been incorporated via the Glauber spin-flip mechanism [38]. In this method, a randomly chosen spin is tried for a change in sign which is accepted according to the standard Metropolis algorithm [37]. We apply periodic boundary conditions in all directions. Time is expressed in units of MC steps (MCS), each MCS consisting of L^d trials, L being the linear dimension of a square or cubic box. We have computed ℓ from the domain size distribution, $P_d(\ell_d, t)$, as [15]

$$\ell(t) = \int \ell_d P_d(l_d, t) d\ell_d, \tag{4}$$

where ℓ_d is calculated as the distance between two successive interfaces along any direction. All lengths are expressed in units of the lattice constant a. We present the results after averaging over multiple initial configurations. This number ranges from 20 (for $L = 1024$) to 200 (for $L = 400$) in $d = 2$ and from 10 (for $L = 256$) to 50 (for $L = 64$) in $d = 3$. The initial configurations for T_i close to T_c were carefully prepared via very long runs. At T_c, for $d = 2$, depending upon the system size, length of such runs varied between 5×10^6 to 10^8 MCS.

3 Results

In this section we present the MC results and their analyses, first from $d = 2$ (Sect. 3.1), followed by $d = 3$ (Sect. 3.2).

3.1 d = 2

Growth of the domains have been demonstrated in the upper frames of Figure 1 for the system size $L = 512$ in $d = 2$. There we show snapshots from two different times during the evolution of the Glauber Ising model. In the lower frames of the figure, we show pictures marking only the persistent spins. Beautiful patterns are visible. These results correspond to a quench from $T_i = \infty$ to the final temperature $T_f = 0$.

Plots of P, for $T_i = \infty$ and few different values of T_f, vs. t, are shown in Figure 2. The data for $T_f = 0$ and $0.25T_c$ are consistent with each other and follow power-law, the exponent being $\theta \simeq 0.22$. The flat behavior at the end is due to the finite-size effects. This value of θ is consistent with the previous observations [20,21]. However, for

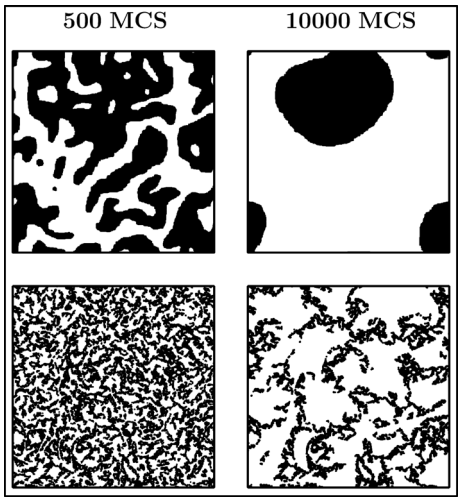

Fig. 1. Upper panels show snapshots during the evolution of the Glauber Ising model with $T_i = \infty$, $T_f = 0$ and $L = 512$. The black regions represent domains of up spins. The lower panels show the unaffected spins, marked in black, corresponding to the evolution snapshots above them. These results correspond to $d = 2$.

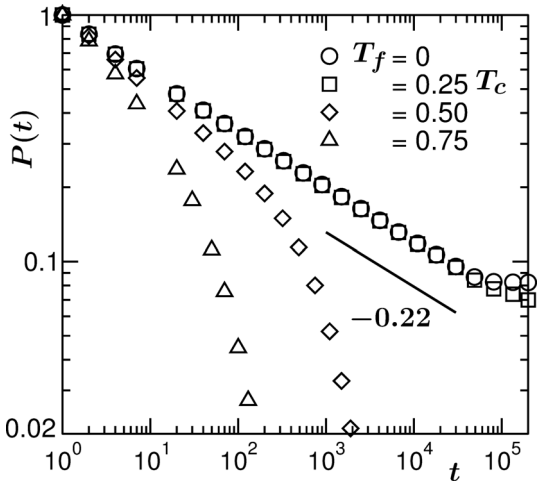

Fig. 2. Plots of persistence probability P vs. time, on a log-log scale, for quenches from $T_i = \infty$, with $L = 512$, in $d = 2$. Four different values of T_f are included. The solid line there has a power-law decay with exponent 0.22.

higher values of T_f, as also previously observed [18,19], the decay is not of power-law type. This is thought to be due to thermal fluctuation. When this fluctuation is taken care of, via the method described below, we observe $\theta \simeq 0.22$ for all the values of T_f included in Figure 2, in agreement with reference [20]. In zero temperature situation spin-flips are related to the motion of the domain boundaries, leading to the growth of ℓ. At nonzero temperature, on the other hand, thermal noise causes flips in the bulk of the domains as well. Following Derrida [19], counting of these bulk spins was discarded by simulating an ordered configuration. In this method, flips common between the original (coarsening) system and the ordered

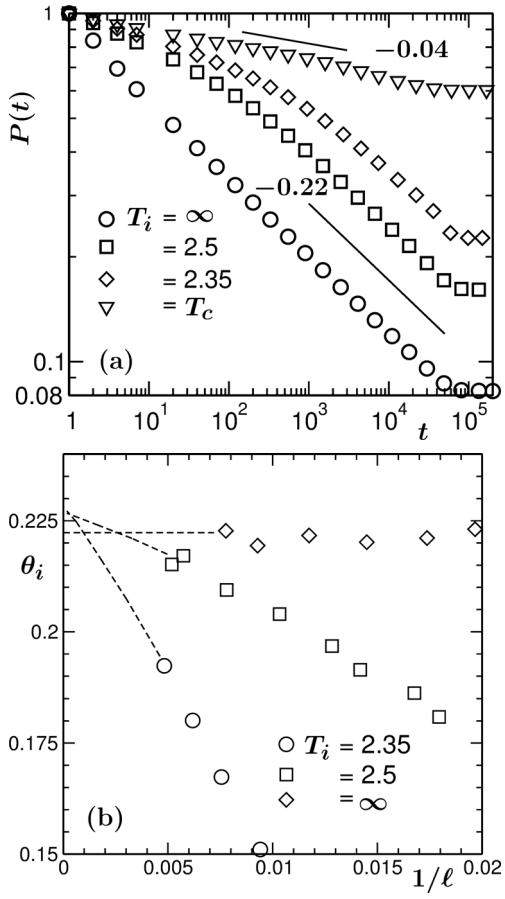

Fig. 3. (a) Log-log plots of P vs. t, for quenches from different values of T_i ($\geqslant T_c$), to $T_f = 0$. Continuous lines there correspond to power-law decays with exponents 0.22 and 0.04. (b) Instantaneous exponents θ_i are plotted vs. $1/\ell$, for the quenches in (a), excluding $T_i = T_c$ case. Here we have included only the late time behavior. The dashed lines in this figure are guides to the eyes. All results are from simulations in $d = 2$.

system were identified as part of bulk dynamics and thus were subtracted from the total number of flips, to stay only with the effects of boundary motion.

It is thought that persistence and domain growth are not strongly connected to each other. Interestingly, different behavior in Figure 2 for $T_f > 0.25T_c$ and $T_f < 0.25T_c$ is strongly reflected in the domain growth also. Essentially a faster early time growth is observed for $T_f \lesssim 0.25T_c$. This we will briefly discuss later.

In Figure 3a we show P vs. t plots, on a log-log scale, for quenches to $T_f = 0$, from a few different values of T_i, all for the same system size $L = 512$. It appears that, in the long time limit, for $T_i > T_c$, the decay is power-law, with the same exponent $\theta \simeq 0.22$. Crossover to this exponent gets delayed as T_i approaches T_c. In the pre-crossover regime, another power-law decay, with smaller exponent, to be represented by $\theta_{\rm I}$, becomes prominent with the decrease of T_i. Such a slower decay becomes ever-lived for $T_i = T_c$. The exponent for the latter case will be denoted by θ_c [$= \theta_{\rm I}(T_i = T_c)$].

In Figure 3b, we present the instantaneous exponent, θ_i, calculated as [14,15]

$$\theta_i = -\frac{d \ln P}{d \ln t}, \tag{5}$$

vs. $1/\ell$, with the objective of accurate quantification of the second step of the decays for T_i close to, but greater than, T_c. For the abscissa variable we have adopted $1/\ell$, instead of $1/t$, to visualize the long time limit better. This is due to the fact that when plotted vs. $1/t$, overall abscissa range increases which makes appreciation of an extrapolation difficult for the data sets corresponding to lower T_i. Within statistical error, for all the presented temperatures, it appears that the values of θ are consistent with that for the quench from $T_i = \infty$ to $T_f = 0$. From this exercise we conclude $\theta = 0.225 \pm 0.005$.

Next we move to identify the exponent for $T_i = T_c$ and $T_f = 0$. In Figure 3a, it appears that the $T_i = T_c$ data are reasonably consistent with $\theta_c = 0.04$. Nevertheless, before the final finite-size effects appear (showing flat nature at very late time), there is a faster decay, albeit for a brief period. This can well be due to the fact that for a finite system, ξ is not infinite at $T = T_c$, effectively implying that the initial configurations are prepared away from T_c. Thus, in this problem, finite-size effects have two sources. One coming from the finiteness of the equilibrium correlation length, other being faced when the nonequilibrium domain size is close to the system size. Thus, a quantification of the exponent θ_c via finite-size scaling [39] becomes a challenging task. However, we appropriately take care of the shortcoming below, in various different ways which provide results consistent with each other.

In Figure 4a we show the instantaneous exponents θ_i, vs. $1/\ell$, with the objective of quantifying the first step of the decays, for two values of T_i, close enough to T_c. As demonstrated, from the flat regions we identify the exponent $\theta_{\rm I}$, which exhibits T_i dependence. These numbers are plotted in the inset of this figure as a function of $\epsilon = T_i - T_c$. The continuous line there is a fit to the form

$$\theta_{\rm I}(T_i) = \theta_c + A\epsilon^x, \tag{6}$$

providing $\theta_c = 0.034$, $A = 0.15$ and $x = 0.54$. Recall that θ_c is the only decay exponent for $T_i = T_c$.

To verify the above value of θ_c further, in Figure 4b we present an exercise with different system sizes. In the main frame of this figure, we present P vs. t data, for $T_i = T_c$, from two different values of L. It is seen that with the increase of the system size, there is a tendency of the data to settle down to a power-law for a longer period of time, following a marginally faster decay at very early time. In the upper inset of this figure we show θ_i vs. $1/\ell$ for three different system sizes with $T_i = T_c$. The early time behavior appears linear, extrapolation of which leads to $\theta_c \simeq 0.029$. However, if the data in the main frame is closely examined, as already mentioned above, this part corresponds to the preasymptotic behavior, thus, should be discarded from the analysis. Actual exponents should be extracted from the flat regions of the plots. In these plots of θ_i vs. $1/\ell$, the flat portions appear very short. But

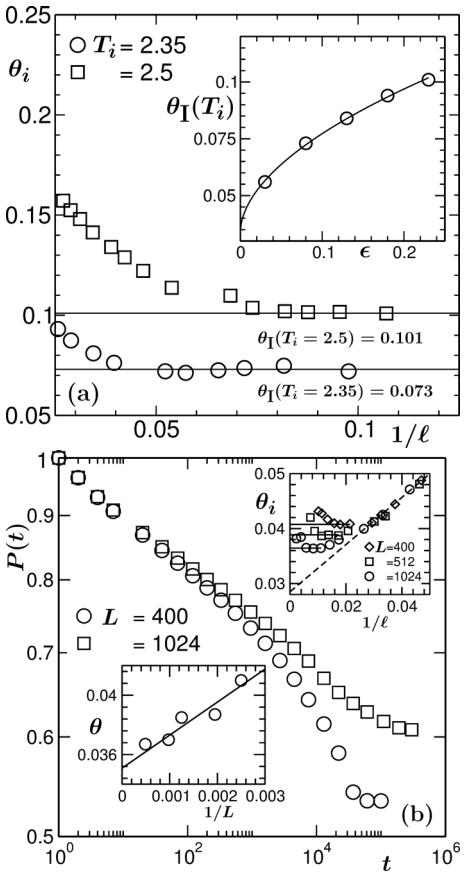

Fig. 4. (a) Instantaneous exponents θ_i are plotted vs. $1/\ell$ for two of the quenches in Figure 3a. Here we have focussed on the first step of the decays, exponents for which are obtained from the flat regions, marked by the horizontal solid lines. These values of θ_I are plotted vs. $\epsilon = T_i - T_c$, in the inset of the figure. The continuous line there is a power-law fit (see text). (b) Plots of P vs. t, for two different system sizes, with $T_i = T_c$ and $T_f = 0$. The upper inset shows θ_i vs. $1/\ell$ for three different values of L, with $T_i = T_c$. The dashed line in this inset is a linear extrapolation using data in the small ℓ region. The L-dependent exponents, $\theta_c(L)$, obtained from flat regions of the plots (see the horizontal solid lines) are plotted vs. $1/L$ in the lower inset. The solid line there is a linear fit. All results correspond to $d = 2$.

the actual time (or length) range over which the flat behavior, before deviating due to finite-size effects, extends, is reasonably long, say, a few hundred MCS for the largest system size. The numbers obtained from these flat parts, as discussed, differs due to the finite-size effects and thus, should be extrapolated to $L = \infty$ appropriately. These L-dependent values, $\theta_c(L)$, are plotted in the lower inset as a function of $1/L$. A very reasonable linear fit (see the solid line) is obtained, providing $\theta_c = \theta_c(L = \infty) = 0.035$. On the other hand, a nonlinear fit (by adding a quadratic term) provides $\theta_c = 0.037$. From all these exercises we conclude that $\theta_c = 0.035 \pm 0.005$. This picture remains true for quenches from T_c to nonzero values of T_f as well, if thermal fluctuation effects are appropriately taken care of. On this issue of thermal fluctuation, here, as well as for

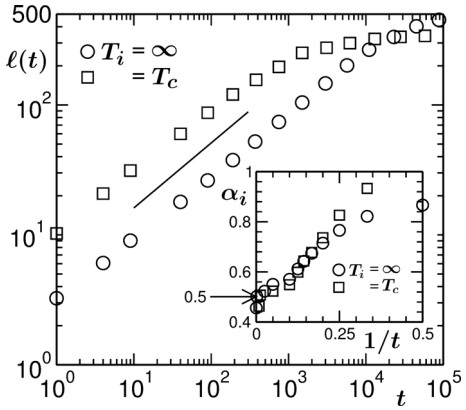

Fig. 5. Average domain sizes, $\ell(t)$, are plotted vs. t, for quenches to $T_f = 0$ from $T_i = \infty$ and T_c, in $d = 2$. The solid line represents $t^{1/2}$ behavior. Corresponding instantaneous exponents, vs. $1/t$, are shown in the inset. All these results are for $L = 512$. For α_i, long time limit data, suffering from strong finite-size effects, have been discarded.

$T_i = \infty$, our conclusions are based on studies with small system sizes. The above quoted value is extremely close to the conclusion from a recent study [35] of the same model on triangular lattice. This implies, the lattice structure plays insignificant role.

The decay of the previously mentioned two-time correlation is also of power-law type. For quenches from $T_i = T_c$, the value of the exponent for this quantity in $d = 2$ gets reduced by a factor $\simeq$10, compared to $T_i = \infty$. In the present case the reduction factor is $\simeq$6.3. While there may be connection between the two phenomena, but a search for matching between the two factors may not be justified. As we will see, this reduction factor is much smaller in $d = 3$, which is consistent with the corresponding prediction for aging dynamics [34].

It is certainly relevant to ask, if, like the decay of the persistence probability and the two-time correlation [33], the growth of the average domain size also exhibits initial temperature dependence. While it is expected [32–34,36] that the long time behavior will be similar, there may be difference at the transient level. For this quantity we make direct examination only for the cases $T_i = \infty$ and $T_i = T_c$, for quenches to $T_f = 0$. Conclusion drawn from these cases will be indirectly shown to be true for other T_i values later.

In Figure 5 we present the ℓ vs. t plots for these two cases, using a log-log scale. Both the data sets appear to grow slower than $t^{1/2}$, even if marginally. This can well be due to the presence of significantly big initial length ℓ_0, which we examine below. While from this figure it is difficult to identify any difference in the growth exponent between the two cases, there certainly exists visible difference in the finite-size effects, noting that $L = 512$ in both the cases.

To learn better about the exponents, in the inset of Figure 5 we present the instantaneous exponents [14,15]

$$\alpha_i = \frac{d \ln \ell}{d \ln t}, \tag{7}$$

with the variation of t. Here, while calculating α_i, we have subtracted ℓ_0 which are $\simeq$2 and $\simeq$6.65, respectively, for $T_i = \infty$ and T_c. This subtraction is meaningful, considering the fact that the pure scaling with respect to time is contained in $\ell - \ell_0$. Calculation of α_i, without such subtraction, provided early time exponents much smaller than the theoretical expectation for the conserved dynamics [14]. This has previously been understood to be due to the curvature dependent correction in small domain size limit. Such confusion has recently been corrected [15]. Note that, there may be a delay time for a system to become unstable following a quench. Thus, for an even more appropriate understanding of a time dependent exponent, the value of ℓ_0 need not be treated as the length at $t = 0$, rather as the (fluctuating) length at which the system falls unstable. Via finite-size scaling analysis, this was demonstrated in a recent work [15]. Here, however, we do not undertake such a task.

For the analysis related to the inset of Figure 5, the value of ℓ_0, as mentioned above, was taken to be that of ℓ at $t = 0$. Thus, ℓ_0 may be identified as ξ at $T = T_i$. Question, however, may be raised that the value of ℓ_0 should then match the system size L for $T_i = T_c$, since ξ is of the order of L at T_c. Note here that, at criticality fluctuations exist at all length scales, giving rise to clusters of all possible sizes, the average, ℓ_0 here, being much smaller than L. These estimates, even though obtained as first moments of the cluster size distributions, are also related to the decay of the two-point correlation functions. The latter function, at the critical point, has power-law decay. The exponential part, that contains information on ξ, is unity at criticality due to diverging value of ξ. Our calculation of ℓ_0 cannot thus be directly related to ξ, particularly close to T_c.

First important observation from the inset of Figure 5 is that the value of α_i approaches 1/2 from the upper side. This fact remains true for $T_f \lesssim 0.25T_c$, as previously mentioned. This is in contrast with the corresponding behavior for the conserved order parameter dynamics with T_f very close to zero [40]. In the latter case, the early time dynamics provides a growth exponent much smaller than the expected asymptotic value 1/3. Second, after $t \simeq 5$, both the data sets practically follow each other, implying no difference in the growth of ℓ almost from the beginning!

From the length (or time) dependence of α_i, one can write

$$\alpha_i = \alpha + f(1/\ell), \tag{8}$$

to obtain

$$\int \frac{d\ell}{\alpha l\left[1 + \frac{1}{\alpha} f(1/\ell)\right]} = \ln t. \tag{9}$$

If $f(1/\ell)$ can be quantified accurately from the simulation data, a full time dependence of ℓ is obtainable. E.g., if $f(1/\ell)$ is a power law, A_β/ℓ^β, A_β being a constant, by taking $\alpha l^\beta > A_\beta$, one finds

$$\ln \frac{\ell^{1/\alpha}}{t} \sim \frac{1}{\alpha^2 \beta \ell^\beta}. \tag{10}$$

Assuming that a correction disappears fast, such that $\ell \simeq t^\alpha$, we obtain

$$\ell \sim t^\alpha \exp\left(-\frac{C}{\alpha\beta t^{\alpha\beta}}\right), \tag{11}$$

C being a constant. Such full forms are useful for a finite-size scaling analysis to accurately quantify the exponent α. It appears that even for a power-law behavior of $f(1/\ell)$, the asymptotic behavior in the growth law can be reached exponentially fast. Of course, from least square fitting exercise of the ℓ vs. t data also one can aim to obtain the early time corrections. However, this method is more arbitrary. Often derivatives help guessing the functional forms better. This full form with the exponential correction factor provided a good fitting to the simulation data from which we obtain α within less than 2% deviation from the expected number 0.5.

Before moving on to presenting results in $d = 3$, we discuss the issue of persistence again. The essential feature in the initial configurations prepared at different temperatures is the variation in the equilibrium correlation length ξ. The basic question, prior to the study, one asks, how does the value of ξ affect the decay of persistence probability? For each value of ξ, do we have a unique exponent describing the full decay? The answer, as we have observed, is certainly not in affirmative. Essentially, the decay exponent for $T_i = \infty$ is recovered for all ξ ($<\infty$) in the long time limit. Only the crossover to this asymptotic behavior gets delayed with the increase of ξ. It is then relevant to ask if this crossover occurs when ℓ crosses ξ, an expectation naturally occurs from renormalization or coarse-graining point of view. Of course a confirmation on this expectation can be obtained from scaling plots (see below) of $P(t)$ by invoking the critical singularity of ξ. However, without detailed knowledge about the finite-size effects of P and ξ, we take an alternative route, by appropriately estimating the crossover length ℓ_c, from the available simulation data.

In the main frame of Figure 6a we show plots of persistence from different values of T_i, for quenches to $T_f = 0$. Here the time axis is scaled by appropriate factors (proportional to cross over time t_c) to obtain collapse of data in the asymptotic regime. Quality of collapse, on top of the $T_i = \infty$ data set, again confirms that $\theta \simeq 0.225$ in the $t \to \infty$ limit for all T_i ($> T_c$). From the square roots of these T_i dependent scaling factors, one can obtain ℓ_c (within a proportionality factor) which is expected to scale as

$$\ell_c \sim \xi \sim \epsilon^{-\nu}. \tag{12}$$

Note that for the Ising model $\nu = 1$ in $d = 2$ and $\simeq$0.63 in $d = 3$. Considering that the $T_i = \infty$ data have been used as the reference case, it will be appropriate to fit the data set for ℓ_c to the form $\ell_c - 1 = A_c\epsilon^{-\nu}$, since (for the current method of estimation) $\ell_c \to 1$ for $T_i = \infty$. Unless we are very close to T_c such additional term cannot be neglected. In the inset of Figure 6a we have plotted $\ell_c - 1$ as a function of ϵ, on a log-log scale. The data set (circles) appear consistent with $\nu = 1$. When ℓ_c is extracted from t_c, a more careful exercise requires incorporation of ℓ_0

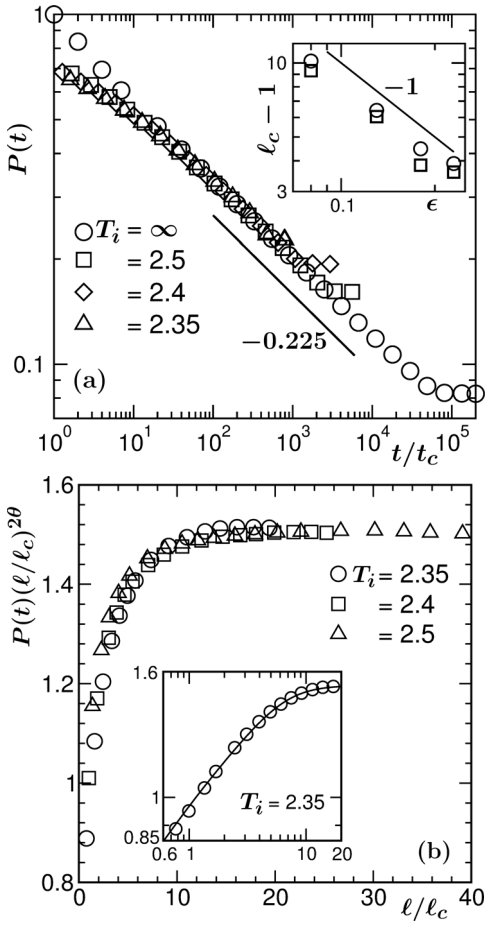

Fig. 6. (a) Scaling plot of persistence probability versus t/t_c where the crossover time (to the asymptotic behavior) t_c has been used as an adjustable parameter to obtain optimum data collapse. Inset: plots of $\ell_c - 1$ vs. ϵ. The circles correspond to estimates of ℓ_c from t_c, the squares are directly obtained from the scaling plots of P vs. ℓ/ℓ_c. The solid line has $d = 2$ Ising critical divergence of correlation length. All results were obtained using $L = 512$ in $d = 2$. (b) Plots of $P(t)(\ell/\ell_c)^{2\theta}$, θ being set to 0.225 (see Fig. 3b), vs. the scaled variable ℓ/ℓ_c, for several values of T_i, using linear scale. Inset: same as the main frame but on a log-log scale and only for $T_i = 2.35$. The continuous line there is a fit to equation (13) (see text for details).

and growth amplitude for each T_i. To avoid this problem, we have also obtained ℓ_c directly from the scaling plots of persistence data vs. ℓ/ℓ_c (see this exercise in Fig. 6b). These values of ℓ_c are represented by squares. Both data sets appear nicely consistent with each other. Least square fittings of these data sets provide $\nu \simeq 0.95$.

As mentioned above, in Figure 6b we show scaling plots of the persistence probability as a function of ℓ/ℓ_c, for three values of T_i. There, in the ordinate, $P(t)$ has been multiplied by $(\ell/\ell_c)^{2\theta}$, the factor 2 in the exponent coming from the expectation that $\alpha = 1/2$ for all values of T_i. For θ, we use 0.225, the value we obtained from the analysis in Figure 3b. The regions of the data sets that suffer from finite-size effects have been carefully discarded. The nice collapse of the data and flat behavior in the long time limit reconfirm the following facts: $\alpha = 1/2$ for all values of T_i and, for $\ell > \ell_c \sim \xi$, in all cases, $P(t)$ decays as $t^{-\theta}$.

It will be interesting to extract the crossover behavior from the transient (first step) to the asymptotic (second step) decay. For this purpose, in the inset of Figure 6b we have plotted the $T_i = 2.35$ data set on a log-log scale, for better visibility of the early time regime. In critical phenomena, in the finite-size scaling analysis of simulation results [41,42], there have been long standing interest in obtaining such crossover functions involving thermodynamic and finite-size limit behaviors. There typically one aims to identify if these two limits are bridged by a power-law or by an exponential function. Along the same line we write

$$P(t)x^{2\theta} = A\left(\frac{x}{g(x)+x}\right)^{\phi};\ x = \ell/\ell_c. \tag{13}$$

For an exponential convergence to the asymptotic behavior we write

$$g(x) = \frac{B_0}{1 + B_1 \exp(B_2 x)}, \tag{14}$$

and for a power-law one

$$g(x) = \frac{C_0}{1 + C_1 x^{\psi}}. \tag{15}$$

In the limit $x \to 0$, $P(t)x^{2\theta} \sim x^{\phi}$, for both the forms of $g(x)$. This limiting behavior was set by considering the fact that for $\ell < \xi$, there exist a power-law decay in $P(t)$ with an exponent $\theta_{\rm I}$, different from θ. For $T_i = 2.35$, this value is $\theta_{\rm I} = 0.073$ (see Fig. 4a). In that case $\phi \simeq 0.304$, taking $\theta = 0.225$. The constant A in equation (13) sets the value of the plateau in the plots of Figure 6b, since for $x \to \infty$, $P(t)x^{2\theta} \to A$. It appears that fit to the power-law form of $g(x)$ looks better and is best for the integral value $\psi = 2$. Other best fit parameters are $A = 1.52$, $C_0 = 3.52$ and $C_1 = 0.033$. The correctness in the value of A can straightway be checked from the figure. The continuous line in the inset of Figure 6b represents the corresponding full function of equation (13). It will be interesting to see if such empirical full form can be confirmed via first principle analytical calculations.

3.2 d = 3

In this subsection we explore $d = 3$. The important facts being discussed in the previous subsection, here we straightway present the results. Noting that nothing remarkable happened for domain growth in the lower dimension, we do not present any direct results for this aspect. However, remarks will be made from indirect analysis.

In Figure 7 we show the P vs. t plots for quenches from $T_i = \infty$ and $T_i = T_c$, keeping $T_f = 0$ in both the cases. For each value of T_i, results from two different system sizes are presented. The data for $T_i = \infty$ are consistent with $\theta = 0.18$, reported previously [20]. Thus, here we aim to accurately quantify the value of θ_c only.

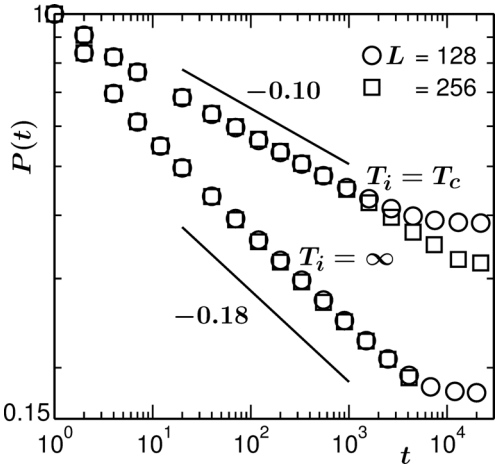

Fig. 7. Plot of P vs. t, for quenches from $T_i = \infty$ and $T_i = T_c$, to $T_f = 0$. In each of the cases, results from two different system sizes are included. The solid lines have power-law decays with exponents 0.1 and 0.18, as indicated on the figure. All results correspond to $d = 3$.

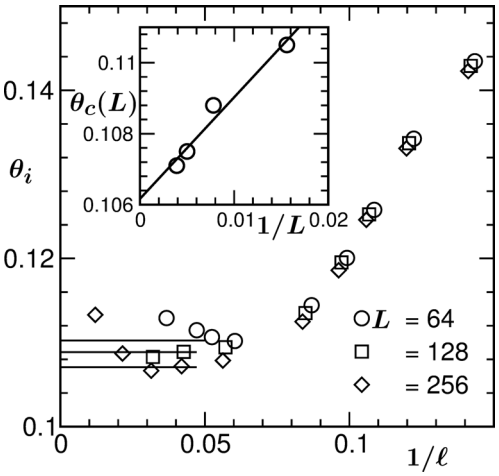

Fig. 8. Instantaneous exponents θ_i are plotted vs. $1/\ell$, for quenches from $T_i = T_c$ to $T_f = 0$ in $d = 3$. Results from different values of L are included. The horizontal solid lines are related to the estimation of L-dependent θ_c. Inset: system size dependent θ_c are plotted as a function of $1/L$. The continuous line there is a linear fitting (see text for details).

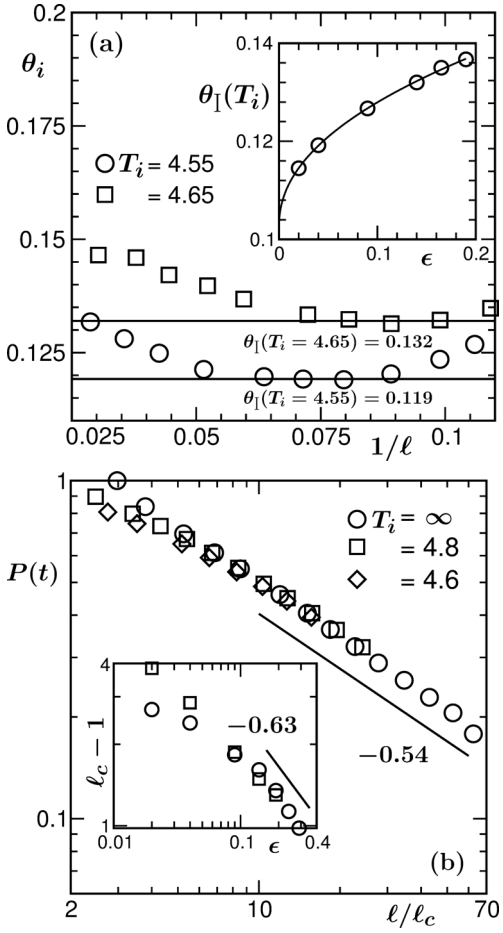

Fig. 9. (a) Estimation of θ_I corresponding to the first step of decay is demonstrated in $d = 3$. Inset: exponent θ_I is plotted as a function of ϵ, in $d = 3$. The continuous line is a non-linear fitting. Further details are provided in the text. Presented results are for $L = 256$. (b) Scaling plot of P vs. ℓ/ℓ_c, in $d = 3$, for $L = 128$. The solid line has a power-law decay with exponent 0.54. Inset: plot of $\ell_c - 1$, in $d = 3$, vs. ϵ. The solid line there has $d = 3$ Ising critical divergence of ξ. We have presented results for $L = 128$ (circles) as well as $L = 256$ (squares).

Even though, for $T_i = T_c$, data from both the system sizes in Figure 7 look consistent with each other, finite-size effects are detectable from a closer look. In the main frame of Figure 8 we plot θ_i versus $1/\ell$ for a few different values of L. Like in $d = 2$, from the flat regions we identify system size dependent θ_c, a plot of which is shown in the inset of this figure. Again, the $\theta_c(L)$ vs. $1/L$ data exhibits a reasonable linear trend and an extrapolation to $L = \infty$ provides $\theta_c = \theta_c(L = \infty) \simeq 0.106$.

Similar to $d = 2$, for $T_c < T_i < \infty$, two step decays exist in $d = 3$ as well. In the main frame of Figure 9a we have demonstrated the estimation of θ_I corresponding to the first step, for two representative values of T_i. In the inset of Figure 9a we have plotted these exponents as a function of ϵ. A fit of this data set to the form in equation (6) provides $\theta_I(T_i = T_c) = \theta_c = 0.103$, $A = 0.074$ and $x = 0.47$. Note the similarity in the values of x in $d = 2$ and 3. This value of θ_c is in good agreement with the one obtained from Figure 8. In $d = 3$, we quote $\theta_c = 0.105 \pm 0.005$. Thus, the effect of growing correlation length in the initial configurations certainly appears weaker in this space dimension. Even though, in both $d = 2$ and 3, fits to the power-law form in equation (6) appear good, due to the similarity of the values in different dimensions, x cannot be connected to any of the other exponents, ν and α, used in this paper, in a simple way. In this work, thus, we treat this exercise only as a reasonably accurate numerical analysis whose validity is justified by the fact that the derivatives of the corresponding simulation data sets, with respect to ϵ, in both dimensions, provide linear looks on double-log plots.

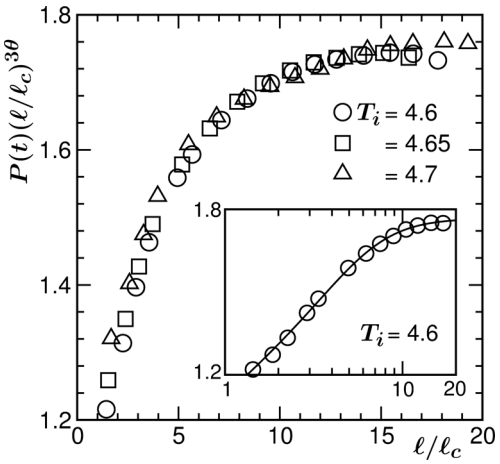

Fig. 10. $P(t)(\ell/\ell_c)^{3\theta}$, with $\theta = 0.18$, are plotted vs. ℓ/ℓ_c, for quenches from three values of T_i to $T_f = 0$, in $d = 3$, using linear scale. Inset: Log-log plot of $P(t)(\ell/\ell_c)^{3\theta}$ vs. ℓ/ℓ_c for $T_i = 4.6$. The continuous line is a fit to the function in equation (13). Further details are provided in the text.

In Figure 9b we show scaling plots of P vs. ℓ/ℓ_c, using data from different values of T_i, with $L = 128$. Collapse of data is again good. The late time behavior is power-law and is consistent with a decay exponent 0.54. Considering that $\theta \simeq 0.18$ in $d = 3$, this implies $\alpha = 1/3$ in $d = 3$. The nice collapse of data sets in Figure 9b, for all values of T_i, implies the initial configuration independence of this exponent. As stated in reference [43], deviation of α, in this dimension, from 1/2, is not yet understood. To avoid this fact, as well as to get rid of the influence of T_i dependent ℓ_0 and growth amplitude, we have obtained ℓ_c from these plots only and no attempts have been made to extract it from scaling plots vs. t/t_c.

In the inset of Figure 9b we plot $\ell_c - 1$ as a function of ϵ, on a log-log scale, for two different system sizes. The divergence of the length scale is consistent with a power law exponent 0.63 which is the critical exponent for ξ in $d = 3$. The deviation from this exponent at smaller values of ϵ is due to finite-size effects. It is clearly seen that for the bigger system ($L = 256$) the effects are much less pronounced. Note that in $d = 3$ it is extremely time consuming to deal with bigger systems, including initial configuration preparation at $T_i = T_c$. To save time for the preparation of initial configuration, in this dimension we have used a combination of Wolff algorithm [44] and Glauber kinetics. In both $d = 2$ and 3, behavior of ℓ_c, as a function of ϵ, have been analyzed for T_i values deviating by maximum of 10% from T_c.

An exercise similar to Figure 6b is shown in Figure 10, for $d = 3$. In this case the exponent on the ordinate is 3θ, instead of 2θ. This is due to a different value of α in the present dimension. Here also we see nice collapse for all the three sets of data we have presented. In the inset we do the exercise related to the crossover function, using $T_i = 4.6$ data set. Here the value of ϕ was set to 0.17, in accordance with the first step of the decay. Again a power-law form of $g(x)$ with the integral value of $\psi = 2$ provides best fit, with other parameters being $A = 1.76$, $C_0 = 12.46$ and $C_1 = 0.055$. Corresponding full function is represented by the continuous line in the inset.

In both $d = 2$ and 3, expectation from coarse-graining point of view that when ℓ exceeds the value of $\xi(T_i)$, $P(t)$ decays with the exponent θ, has been confirmed. In the present case, the value of ξ at T_f is zero. It remains to be seen how $\xi(T_f)$, for $T_f \neq 0$, interferes with the crossover. Even though we have studied cases where both $\xi(T_i)$ and $\xi(T_f)$ are nonzero, this particular aspect requires more careful study.

4 Conclusions

In conclusion, we have studied phase ordering dynamics in Ising ferromagnets for various combinations of initial (T_i) and final (T_f) temperatures in $d = 2$ and 3. In this work, the primary focus has been on the persistence probability, P, and its connection with the growth of average domain size, ℓ, as well as with the equilibrium initial correlation length ξ.

Our general observation has been that, irrespective of the value of T_i, the decay of P becomes faster with the increase of T_f, after a certain critical number for the latter. This is understood to be due to spins affected by thermal fluctuations. When this effect is taken care of [19], the long time decay appears to be power law with exponent [20,21] consistent with the one for quench to $T_f = 0$.

As T_i approaches T_c, two-step power-law decay becomes prominent, the second part having exponent $\theta \simeq 0.225$ in $d = 2$ and $\simeq 0.18$ in $d = 3$, same as $T_i = \infty$ and $T_f = 0$ case. For $T_i = T_c$, thought to provide a new universality class, the first part of the two-step process lives for ever. The corresponding values of the exponent have been identified to be $\theta_c \simeq 0.035$ in $d = 2$ and $\theta_c \simeq 0.105$ in $d = 3$. Thus the decay of persistence probability is strongly connected with the initial correlation length. It has been shown that the crossover length to the second step of decay diverges as the equilibrium correlation length in both the dimensions. This leads to the question of difference in the fractal dimensions in the pre- and post-crossover regimes. Our preliminary study in this respect confirms the expectation that, for finite T_i, in the post-crossover regime only the fractal dimension is same as the $T_i = \infty$ case. We have also estimated the crossover function between the two steps. It appears, a convergence to the asymptotic decay occurs in a power-law manner, as a function of ℓ/ξ.

We have not observed any initial configuration dependence of the growth of the average domain size. This is consistent with a previous study [36] but more explicitly demonstrated here. Essentially, even the transients are only weakly affected due to change in initial temperature. However, stronger finite-size effects are detected for lower values of T_i. For domain growth, a striking observation is that the early time exponent is much higher than the asymptotic value, despite T_f being zero. This is at variance with the conserved order parameter dynamics. These are all interesting new results, requiring appropriate theoretical attention.

In future we will focus on persistence for the conserved order parameter dynamics. For the conserved dynamics, initial temperature dependence of aging and domain growth are also important open problems.

The authors acknowledge useful discussion with S.N. Majumdar and are thankful to the Department of Science and Technology, India, for financial support via grant number SR/S2/RJN-13/2009. S.K.D. is thankful to International Centre for Theoretical Physics, Italy, for hospitality and financial support. The authors have equal contributions.

References

1. A. Onuki, *Phase Transition Dynamics* (Cambridge University Press, Cambridge, 2002)
2. S. Puri, V. Wadhawan, *Kinetics of Phase Transitions* (Boca Raton, CRC Press, 2009)
3. A.J. Bray, Adv. Phys. **51**, 481 (2002)
4. K. Binder, in *Phase Transformation of Materials*, edited by P. Haasen, *Materials Science and Technology* (VCH, Weinheim, 1991), Vol. 5, p. 405
5. M.C. Cross, P.C. Hohenberg, Rev. Mod. Phys. **65**, 851 (1993)
6. T. Ohta, D. Jasnow, K. Kawasaki, Phys. Rev. Lett. **49**, 1223 (1982)
7. A.J. Bray, S. Puri, Phys. Rev. Lett. **67**, 2670 (1991)
8. H. Toyoki, Phys. Rev. B **45**, 1965 (1992)
9. S.K. Das, S. Puri, M.C. Cross, Phys. Rev. E **64**, 46206 (2001)
10. I.M. Lifshitz, V.V. Slyozov, J. Phys. Chem. Solids **19**, 35 (1961)
11. K. Binder, D. Stauffer, Phys. Rev. Lett. **33**, 1006 (1974)
12. S.M. Allen, J.W. Cahn, Acta Metall. **27**, 1085 (1979)
13. E.D. Siggia, Phys. Rev. A **20**, 595 (1979)
14. D.A. Huse, Phys. Rev. B **34**, 7845 (1986)
15. S. Majumder, S.K. Das, Phys. Rev. E **81**, 050102 (2010)
16. S.N. Majumdar, C. Sire, A.J. Bray, S.J. Cornell, Phys. Rev. Lett. **77**, 2867 (1996)
17. S.N. Majumdar, A.J. Bray, S.J. Cornell, C. Sire, Phys. Rev. Lett. **77**, 3704 (1996)
18. B. Derrida, V. Hakim, R. Zeitak, Phys. Rev. Lett. **77**, 2871 (1996)
19. B. Derrida, Phys. Rev. E **55**, 3705 (1997)
20. D. Stauffer, Int. J. Mod. Phys. C **8**, 361 (1997)
21. G. Manoj, P. Ray, Phys. Rev. E **62**, 7755 (2000)
22. D. Chakraborty, J.K. Bhattacharjee, Phys. Rev. E **76**, 031117 (2007)
23. M. Saharay, P. Sen, Physica A **318**, 243 (2003)
24. R. Paul, A. Gambassi, G. Schehr, Europhys. Lett. **78**, 10007 (2007)
25. A.J. Bray, S.N. Majumdar, G. Schehr, Adv. Phys. **62**, 225 (2013)
26. D.S. Fisher, D.A. Huse, Phys. Rev. B **38**, 373 (1988)
27. F. Liu, G.F. Mazenko, Phys. Rev. B **44**, 9185 (1991)
28. F. Corberi, E. Lippiello, M. Zannetti, Phys. Rev. E **74**, 041106 (2006)
29. S. Ahmad, F. Corberi, S.K. Das, E. Lippiello, S. Puri, M. Zannetti, Phys. Rev. E **86**, 061129 (2012)
30. S. Majumder, S.K. Das, Phys. Rev. Lett. **111**, 055503 (2013)
31. J. Midya, S. Majumder, S.K. Das, J. Phys.: Condens. Matter **26**, 452202 (2014)
32. C. Dasgupta, R. Pandit, Phys. Rev. B **33**, 4752 (1986)
33. K. Humayun, A.J. Bray, J. Phys. A **24**, 1915 (1991)
34. A.J. Bray, K. Humayun, T.J. Newman, Phys. Rev. B **43**, 3699 (1991)
35. T. Blanchard, L.F. Cugliandolo, M. Picco, J. Stat. Mech. Theor. Exp. **2014**, P12021 (2014)
36. A. Sicilia, J.A. Arenzon, A.J. Bray, L.F. Cugliandolo, Phys. Rev. E **76**, 061116 (2007)
37. D.P. Landau, K. Binder, *A Guide to Monte Carlo Simulations in Statistical Physics* (Cambridge University Press, Cambridge, 2009)
38. R.J. Glauber, J. Math. Phys. **4**, 294 (1963)
39. M.E. Fisher, in *Critical Phenomena*, edited by M.S. Green (Academic Press, London, 1971)
40. S. Majumder, S.K. Das, Phys. Chem. Chem. Phys. **15**, 13209 (2013)
41. *Finite Size Scaling and Numerical Simulation of Statistical Systems*, edited by V. Privman (World Scientific, 1990)
42. S.K. Das, M.E. Fisher, J.V. Sengers, J. Horbach, K. Binder, Phys. Rev. Lett. **97**, 25702 (2006)
43. S. Cueille, C. Sire, J. Phys. A **30**, L791 (1997)
44. U. Wolff, Phys. Rev. Lett. **62**, 361 (1989)